

000 001 002 003 004 005 REGUIDE: DATA EFFICIENT GUI GROUNDING VIA 006 SPATIAL REASONING AND SEARCH 007 008 009

010 **Anonymous authors**
011 Paper under double-blind review
012
013
014
015
016
017
018
019
020
021
022
023
024
025
026

ABSTRACT

027 Recent advances in Multimodal Large Language Models (MLLMs) have enabled
028 autonomous agents to interact with computers via Graphical User Interfaces (GUIs),
029 where accurately localizing the coordinates of interface elements (e.g., buttons)
030 is often required for fine-grained actions. However, this remains significantly
031 challenging, leading prior works to rely on large-scale web datasets to improve the
032 grounding accuracy. In this work, we propose Reasoning Graphical User Interface
033 Grounding for Data Efficiency (ReGUIDE), a novel and effective framework for
034 web grounding that enables MLLMs to learn data efficiently through self-generated
035 reasoning and spatial-aware criticism. More specifically, ReGUIDE learns to (i)
036 self-generate a language reasoning process for the localization via online reinforce-
037 ment learning, and (ii) criticize the prediction using spatial priors that enforce
038 equivariance under input transformations. At inference time, ReGUIDE further
039 boosts performance through a test-time scaling strategy, which combines spatial
040 search with coordinate aggregation. Our experiments demonstrate that ReGUIDE
041 significantly advances web grounding performance across multiple benchmarks,
042 outperforming baselines with substantially fewer training data points (that is, only
043 0.2% samples compared to the best open-source baselines).
044

1 INTRODUCTION

045 Graphical User Interface (GUI) agents—i.e., Multimodal Large Language Model (MLLM) agents
046 that interpret visual screen contents and generate web actions in natural language to navigate the web
047 environment—have shown promising capabilities in web navigation tasks as MLLMs continue to
048 improve in general decision-making ability (OpenAI, 2024; Anthropic., 2024; Qin et al., 2025; Zheng
049 et al., 2024). Despite the recent significant efforts, however, a substantial gap remains between the
050 performance of these agents and that of proficient human users (Chen et al., 2025), particularly in
051 complex or long-horizon tasks (Zhang et al., 2025). This gap arises mainly from two challenges:
052 limited visual understanding of web pages (Wang et al., 2024) and insufficient web domain-specific
053 decision-making ability (Gou et al., 2024). To address this, prior work typically decomposes the
054 problem into two parts: (i) building an MLLM that can interpret the visual input (Zheng et al., 2024)
055 and (ii) employing a language model that performs decision-making and planning based on the
056 MLLM’s interpretation (Qin et al., 2025; Hong et al., 2024), where the major bottleneck lies in the
057 visual understanding component (Gou et al., 2024).
058

059 Building an MLLM that can predict the exact pixel coordinates of target region on the screen (e.g.,
060 buttons) has shown great promise in providing the visual understanding required by another LLM for
061 effective decision-making (Gou et al., 2024). However, grounding remains challenging as it requires
062 fine-grained skills such as reasoning and the manifestation of spatial understanding (Ma et al., 2025;
063 Zhao et al., 2025). Recent approaches have emphasized the importance of large-scale, high-quality
064 image–instruction pairs for training MLLMs through supervised fine-tuning (SFT) (Lin et al., 2024;
065 Gou et al., 2024). Gou et al. (2024) proposes synthesizing diverse referring expressions that can
066 express the same object in several views. However, such SFT models depend on costly data curation
067 to perform well, which poses a major scalability challenge (Huang et al., 2025).
068

069 To this end, we focus on extracting rich information from web image data to achieve data-efficient
070 grounding by learning to explain the coordinate prediction process in natural language and by
071 leveraging spatial priors to maximize the utility of visual input.
072

054 **Contribution.** We propose Reasoning Graphical User Interface Grounding for Data Efficiency
 055 (ReGUIDE), a novel and effective GUI coordinate grounding method for web agents. Specifically,
 056 ReGUIDE is composed of a two-stage training: (i) self-generation of image explanation through its
 057 own reasoning, and (ii) criticism of the localization prediction via spatial priors. First, ReGUIDE
 058 learns to generate the language description of the given web image that can guide itself to correctly
 059 predict the coordinate, where this prediction accuracy is used as the reward for online RL. Then,
 060 by leveraging a spatial prior—i.e., the fact that augmentations such as cropping lead to equivariant
 061 changes in the target coordinates—the model criticizes its predictions by ensuring consistent outputs
 062 under the same language description across augmented image–coordinate pairs.

063 Furthermore, we introduce an inference-time scaling strategy for ReGUIDE, which integrates spatial
 064 search. Specifically, the model generates multiple localization predictions and crops the region where
 065 the target is likely to exist based on the predictions. In this region, we generate multiple coordinate
 066 candidates, then aggregate the candidates into a single coordinate via statistical voting strategy (i.e.,
 067 Kernel Density Estimation (Rosenblat, 1956) (KDE)-based voting).

068 We demonstrate the effectiveness of ReGUIDE through evaluations on multiple web-grounding
 069 datasets and agent-setting benchmarks. Notably, ReGUIDE enhances web coordinate grounding
 070 performance beyond prior methods, achieving the state-of-the-art performance in web grounding.
 071 For instance, ReGUIDE improves the grounding accuracy of Qwen-2.5-VL-3B from 55.5% to 87.3%
 072 on SCREENSPOT (CHENG ET AL., 2024A) and from 23.9% to 44.3% on SCREENSPOT-PRO (LI
 073 ET AL., 2025). Moreover, our experimental results show that ReGUIDE indeed guides the GUI agent
 074 to improve the overall decision-making ability, showing a significant performance improvement in
 075 agentic tasks. Beyond demonstrating the overall effectiveness of ReGUIDE, we further analyze the
 076 contribution of each component and show how they individually enhance grounding performance.

077 2 RELATED WORK

080 **Graphic User Interface (GUI) grounding.** Recent advances in pixel-level GUI grounding have
 081 demonstrated mapping natural language instructions to screen coordinates without relying on HTML
 082 or DOM structures (Shaw et al., 2023). Several prior works (Xu et al., 2024; Wu et al., 2024;
 083 Cheng et al., 2024b; Lin et al., 2024) train on over a million synthesized screenshots and achieve
 084 superior performance. Gou et al. (2024) and Yang et al. (2025b) further shows that synthesizing
 085 and augmenting text instructions can lead to further improvements. However, current approaches
 086 depend on massive annotated datasets, incurring substantial computation and labeling costs, and
 087 neither leverages the reasoning capabilities of large language models to improve localization under
 088 data-scarce or out-of-distribution conditions.

089 **Reinforcement learning in MLLM.** Reinforcement learning has emerged as a powerful mechanism
 090 to fine-tune multimodal large language models (MLLMs) via self-improvement and feedback. Self-
 091 Critical Sequence Training (Rennie et al., 2017) researched policy-gradient optimization for image
 092 captioning. RLHF-V (Yu et al., 2024) formulates multimodal RLHF under constrained optimization
 093 to jointly maximize helpfulness and minimize unsafe outputs. More recently, Vision-R1 (Huang et al.,
 094 2025) generates reasoning trajectories and applies iterative policy optimization to boost multimodal
 095 math reasoning. For GUI grounding, several concurrent RL-based approaches (Lu et al., 2025;
 096 Xia & Luo, 2025; Lian et al., 2025; Yuan et al., 2025; Yang et al., 2025a) optimize grounding
 097 decisions via reinforcement learning, often emphasizing dataset curation, and reward shaping. In
 098 contrast, ReGUIDE takes a fundamentally different perspective which focus on leveraging spatial
 099 priors through transformation consistency training and test-time spatial search rather than reward
 100 design. These components can be operate agnostically for existing models, ReGUIDE can be applied
 101 orthogonally to existing models and improve performance generally as shown in Table 1 and Table 2

102 **Test-time scaling.** Recent works explored that scaling test-time computation, such as best-of-N
 103 sampling, can be even better than scaling train-time computation for performance (Snell et al., 2024).
 104 Specifically, test-time scaling strategies improve LLM performance by generating numerous candidate
 105 outputs and selecting the best (Snell et al., 2024; Lee et al., 2025; Hosseini et al., 2024). To enhance
 106 decision-making, external verifiers are often employed to evaluate and refine these outputs (Hosseini
 107 et al., 2024). In the localization task, recent work framed the localization as a search problem and
 108 suggested a test-time scalable strategy (Wu & Xie, 2024; Luo et al., 2025). Unlike prior approaches
 109 that only aggregate predictions by selecting the most confident point without proposing any training

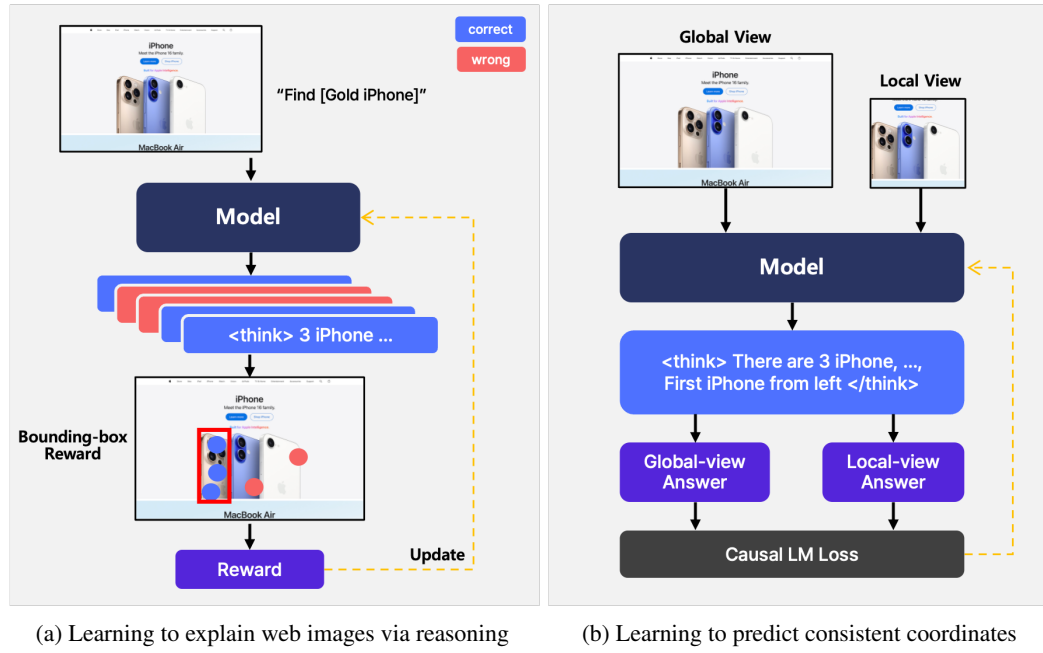


Figure 1: **Overview of training ReGUIDE.** **Left:** The model rolls out multiple (reasoning, coordinate) pairs; rewards the point that falls inside the ground-truth box. **Right:** Trains the model on paired full-image and cropped views, sharing the reasoning tokens while adjusting the coordinate, which provides multi-view consistency and improves grounding performance.

scheme, we additionally introduce a novel learning method and a more advanced aggregation strategy motivated by the Gaussian-shaped likelihood distribution of coordinate tokens observed in Figure 3. As shown in Table 11, this approach enables ReGUIDE to outperform alternative methods.

3 DATA EFFICIENT GUI GROUNDING VIA SPATIAL REASONING AND SEARCH

In this section, we present Reasoning Graphical User Interface Grounding for Data Efficiency (ReGUIDE), a Graphical User Interface (GUI) grounding (i.e., coordinate prediction) training framework that self-generates the language description of the image through reasoning, and criticizes the prediction with spatial priors. We present the core training method in Section 3.1, and then the test-time search method in Section 3.2. The overview of ReGUIDE is depicted in Figure 1.

Problem setup. We describe the problem setup of our interest, namely the GUI grounding: training an MLLM that can predict the coordinate of the interface (e.g., ‘close button’) in the web image based on the given instruction (e.g., ‘close the window’). Formally, given an input instruction x_{inst} and image x_{img} , the MLLM \mathcal{M} generates the output which consists of reasoning path r and predicted coordinate $\mathbf{c} = (c_1, c_2)$, i.e., $r, \mathbf{c} \sim \mathcal{M}(\cdot | x_{\text{inst}}, x_{\text{img}})$. Here, we denote the ground-truth region in the pixel coordinate space corresponding to $(x_{\text{inst}}, x_{\text{img}})$ as $\mathcal{X}_{\text{gt}} \subseteq [0, W] \times [0, H]$, where W and H are the width and height of x_{img} . Any coordinate $\mathbf{c} \in \mathcal{X}_{\text{gt}}$ is considered a correct prediction, as all such points result in the same GUI behavior (e.g., triggering the intended button or link).

3.1 REGUIDE: REASONING GRAPHICAL USER INTERFACE GROUNDING FOR DATA EFFICIENCY

We describe the core training pipeline of ReGUIDE. The key idea is to extract rich information from web images, enabling the model to generalize even with a relatively small training dataset. To this end, we train the model to self-explain the reasoning behind its predictions, as learning an explicit reasoning process—rather than merely memorizing input-output patterns—is crucial for generalization (Nye et al., 2021; Lampinen et al., 2022). Building on this learned reasoning, we

162 further refine the predictions through a consistency enforcement step, which assesses the consistency
 163 of the output under image augmentations while maintaining the same reasoning trace.
 164

165 **Learning to explain GUI images via reasoning.** At the first stage, we train the LLM to reason
 166 about the exact coordinate of the instruction on the screen, where we employ online reinforcement
 167 learning (RL) to make MLLM self-evolve by using grounding accuracy as a reward. This enables
 168 the model to generate its own text reasoning and evolve without relying on externally provided
 169 language descriptions, thus saving the language annotation cost. RL also tends to generalize better
 170 than supervised fine-tuning (SFT), which may suffer from memorization (Nye et al., 2021).
 171

172 For a given instruction x_{inst} and an image x_{img} , we define two reward functions to train MLLM
 173 with RL. Specifically, we consider (i) the result of ground truth prediction as the primary reward and
 174 (ii) an auxiliary formatting reward that encourages the model to wrap its reasoning trace between
 175 ‘<think>’ and ‘</think>’ tags, ensuring that the generated reasoning follows the desired format
 176 for downstream usage by following recent work in LLM reasoning (Huang et al., 2025; Guo et al.,
 177 2025). Formally, we define the reward function $R(\cdot, \cdot)$ as follows:

$$R(r, \mathbf{c}) = \mathbf{1}[\mathbf{c} \in \mathcal{X}_{\text{gt}}] + \lambda \cdot \mathbf{1}[\text{format}(r) = <\text{think}> \dots </\text{think}>], \quad (1)$$

178 where $\mathbf{1}[\cdot]$ denotes the indicator function that returns one if the condition holds and zero otherwise,
 179 $\text{format}(r)$ extracts the outermost structure of the generated reasoning trace to check whether it
 180 is properly enclosed between $<\text{think}>$ and $</\text{think}>$, and $\lambda \in \mathbb{R}^+$ is a hyperparameter that
 181 balances the contribution of the formatting reward, where we use $\lambda = 0.1$ throughout the experiment.
 182

183 The overall RL objective is to maximize the expected reward:

$$\max_{\mathcal{M}} \mathbb{E}_{x_{\text{inst}}, x_{\text{img}}} \mathbb{E}_{(r, \mathbf{c}) \sim \mathcal{M}(\cdot | x_{\text{inst}}, x_{\text{img}})} [R(r, \mathbf{c})]. \quad (2)$$

184 To this end, we adopt Group Relative Policy Optimization (GRPO) (DeepSeek, 2024) as our RL
 185 algorithm, as GRPO enhances both efficiency and stability by sampling multiple candidate outputs
 186 per input and computing group-relative rewards. This overall process allows the model to explore
 187 diverse reasoning strategies and progressively reinforce those that contribute to accurate grounding,
 188 without relying on explicit reasoning supervision.
 189

190 **Learning to predict consistent coordinates under transformations.** While the RL stage enables
 191 the model to predict coordinates within the correct ground truth region, it does not necessarily guide
 192 the model toward predicting the most precise or stable point, typically the center of the target element
 193 (as the target UI element is annotated with a bounding box, making the center a natural target).
 194 Additionally, the model may be sensitive to variations in scale and cropping, which can degrade
 195 performance in real-world scenarios where UI elements may appear at different sizes or positions.
 196

197 To address these limitations, we introduce a further training phase that enforces spatial precision and
 198 view consistency. Specifically, we continually train the MLLM to predict the center of the ground-
 199 truth region, while jointly enforcing consistent predictions under image transformations through
 200 spatial priors. In particular, we focus on constraining consistency between the model’s predictions on
 201 the global view (full image) and the local view (a zoomed-in crop covering the ground-truth region).
 202 Notably, such global-local view consistency has been identified as a key factor in the success of
 203 prior self-supervised vision methods (Caron et al., 2021; Oquab et al., 2023; Hjelm et al., 2018).
 204 Furthermore, we make the local view follow the reasoning process of the global view (as it typically
 205 contains relative spatial cues), forming a self-distillation of the reasoning process.
 206

207 Formally, we collect two data points, namely the global view data $\mathbf{d}_{\text{global}}$ and local view data
 208 $\mathbf{d}_{\text{local}}$, where each data point consists of image, instruction, reasoning, and target coordinates. Here,
 209 both data points consist of the same instruction and reasoning, but with different images and target
 210 coordinates (due to the spatial transformation). To ensure high-quality reasoning, we repeat the
 211 the sampling 4-time from given reasoning and just select the reasoning which consistently predict
 212 the target region in the global image x_{img} , i.e., select r from $r \sim \mathcal{M}(\cdot | x_{\text{inst}}, x_{\text{img}})$ such that
 213 $\{\mathbf{c}_i\}_{i=0}^3 \sim \mathcal{M}(\cdot | r, x_{\text{text}}, x_{\text{img}}), \wedge_{i=0}^3 \mathbf{c}_i \in \mathcal{X}_{\text{gt}}$. For the global view data, we use the non-
 214 transformed image x_{img} and the center of the ground truth region $\text{center}(\mathcal{X}_{\text{gt}})$, while for the local
 215 view data, we use a randomly cropped image $\text{crop}(x_{\text{img}})$ and the center of the transformed ground
 216 truth region, denoted as $\text{center}(\mathcal{X}_{\text{gt}}^{\text{crop}})$. Namely, the global and local view data are defined as:
 217

$$\mathbf{d}_{\text{global}} := (x_{\text{inst}}, x_{\text{img}}, r, \text{center}(\mathcal{X}_{\text{gt}})), \quad \mathbf{d}_{\text{local}} := (x_{\text{inst}}, \text{crop}(x_{\text{img}}), r, \text{center}(\mathcal{X}_{\text{gt}}^{\text{crop}})).$$

216 For training, the model processes the original global view and the newly created local view in the
 217 same batch, and is supervised via next-token prediction loss to generate the updated coordinates:
 218

$$219 \quad \min_{\mathcal{M}} \mathcal{L}(\mathbf{d}_{\text{global}}) + \mathcal{L}(\mathbf{d}_{\text{local}}), \quad \text{where } \mathcal{L}(\mathbf{d}) = -\log \mathcal{M}(r, \mathbf{c} \mid x_{\text{inst}}, x'_{\text{img}}), \quad (3)$$

220 where $\mathbf{d} = (x_{\text{inst}}, x'_{\text{img}}, r, \mathbf{c})$ and x'_{img} denotes the input image used in the given view (i.e., x_{img} for
 221 the global view and $\text{crop}(x_{\text{img}})$ for the local view).
 222

223 3.2 TEST-TIME SCALING WITH SPATIAL SEARCH AND KDE-BASED AGGREGATION

224 Despite their strong reasoning capabilities via natural text, LLMs inherently struggle with coordinate
 225 prediction due to their limited awareness of ordinal relationships among numeric tokens. To alleviate
 226 the issue, we propose a scalable inference method for trained models. Specifically, we introduce a
 227 two-stage inference method, namely, composed of the **(i) cropping** and the **(ii) voting** stages. Here,
 228 the key idea for each stage is to (i) zoom in on the image where the UI element is likely to exist, and
 229 (ii) predict multiple coordinates, which are finalized to a single coordinate by using Gaussian kernel
 230 density estimation. An illustration of our test-time spatial search strategy is provided in Appendix D.
 231

232 **Cropping: Zooming into the UI element area.** To crop the region where the UI element is likely
 233 to exist, we first predict multiple coordinates on the full image. Then, we treat these predictions
 234 as samples from a probability distribution indicating the target’s likely location. Here, we use
 235 Kernel Density Estimation (KDE) to analyze these initial samples and identify the region of highest
 236 prediction density—the area where the model is most consistently expected to be the target. Thus,
 237 we choose the highest density point as the center of the cropped Region of Interest (RoI), effectively
 238 allowing the model to “zoom in” on the most promising area.
 239

240 Concretely, given an input image x_{img} and instruction x_{inst} , we sample N initial predictions: $\mathcal{C} :=$
 241 $\{\mathbf{c}^{(i)}\}_{i=1}^N$, where $(r^{(i)}, \mathbf{c}^{(i)}) \sim \mathcal{M}(\cdot \mid x_{\text{inst}}, x_{\text{img}})$. Then, we apply KDE to these N predictions to
 242 find the ‘center’ \mathbf{c}_{KDE} of the predictions by summing 2D Gaussian kernels (with a pre-defined variance
 243 Σ) centered at each prediction $\mathbf{c}^{(j)}$ to estimate a density $S(z; \mathcal{C})$:
 244

$$245 \quad \mathbf{c}_{\text{KDE}} = \underset{z \in [0, W] \times [0, H]}{\text{argmax}} S(z; \mathcal{C}) \quad \text{where } S(z; \mathcal{C}) = \mathbb{E}_{\mathbf{c} \in \mathcal{C}} \left[\exp \left(-\frac{1}{2} (z - \mathbf{c})^\top \Sigma^{-1} (z - \mathbf{c}) \right) \right]. \quad (4)$$

246 A fixed-size bounding box \mathcal{X}_{RoI} (with dimensions $W_{\text{RoI}} \times H_{\text{RoI}}$), centered at \mathbf{c}_{KDE} , defines the region
 247 of interest. We crop the image to this region: $\text{RoI}(x_{\text{img}}) = \text{crop}(x_{\text{img}}; \mathbf{c}_{\text{KDE}}, W_{\text{RoI}}, H_{\text{RoI}})$.
 248

249 **Voting: Aggregating multiple votes within RoI.** In the voting stage, we further refine the coordinate
 250 prediction within this RoI. Given the local zoomed-in view, these predictions are expected to be more
 251 precise – the answer space is narrowed. We then reapply KDE to these new predictions within the
 252 RoI. This second application of KDE acts as a robust voting mechanism, aggregating the multiple
 253 refined predictions to determine the single coordinate with the highest probable point (i.e., the peak of
 254 the density). This two-stage searching strategy not only allows ReGUIDE to more precisely predict
 255 the final answer but also offers scalability: investing more computational resources in generating and
 256 evaluating samples for refinement generally leads to a more accurate result.
 257

258 Formally, the model re-predicts M new coordinates: $\mathcal{C}_{\text{RoI}} := \{\mathbf{c}_{\text{RoI}}^{(i)}\}_{i=1}^M$, where $(r^{(i)}, \mathbf{c}_{\text{RoI}}^{(i)}) \sim \mathcal{M}(\cdot \mid$
 259 $x_{\text{inst}}, \text{RoI}(x_{\text{img}}))$. Then, we use the same process as in Equation 4 to predict the most confident
 center point $\mathbf{c}_{\text{final}}$ within $\mathcal{C}_{\text{RoI}} \cup \mathcal{C}$ by robustly aggregating coordinates with KDE:
 260

$$261 \quad \mathbf{c}_{\text{final}} = \underset{z \in \mathcal{X}}{\text{argmax}} S(z; \mathcal{C}_{\text{RoI}} \cup \mathcal{C}). \quad (5)$$

262 4 EXPERIMENTS

263 We provide an empirical evaluation of ReGUIDE by investigating the following questions:
 264

- 265 • Can ReGUIDE enhance GUI grounding performance? (Table 1 and Table 3)
- 266 • Can ReGUIDE improve overall GUI agent performance? (Table 8)
- 267 • How does the MLLM perform reasoning based on the given instruction and image? (Table 4)
- 268 • Do the proposed components enhance the grounding performance? (Table 5 and Table 7)

270 Table 1: Accuracy (%) for ReGUIDE (Ours) and other baselines, for the fair comparison we trained
 271 with same dataset UGround with different data size. We evaluate on three web-grounding benchmarks:
 272 SCREENSPOT (ScrSpot), SCREENSPOT-v2 (ScrSpot-v2), and SCREENSPOT-PRO (ScrSpot-pro).
 273 Models trained with the same dataset but different size (i.e., a 20K subset of UGround, 10M fullset of
 274 UGround) . Bold indicates the best result within each group.

Methods	Data Size	SCRSPOT	SCRSPOT-V2	SCRSPOT-PRO
<i>Trained with same dataset</i>				
UGround-2B (Gou et al., 2024)	10M	77.7	81.4	26.6
UGround-7B (Gou et al., 2024)	10M	86.3	89.1	31.1
Qwen-2.5-VL-3B (Alibaba, 2025)	-	55.5	70.4	23.9
+ SFT	20K	56.8	56.5	11.6
+ ReGUIDE w/o TTS	20K	84.9	87.6	27.9
+ ReGUIDE (Ours)	20K	88.0	90.0	44.5
Qwen-2.5-VL-7B (Alibaba, 2025)	-	84.7	82.6	29.0
+ SFT	20K	84.9	88.9	25.9
+ ReGUIDE w/o TTS	20K	88.1	91.0	36.3
+ ReGUIDE (Ours)	20K	90.2	92.3	47.1

289 Before answering each question, we outline the experimental protocol (more details in Appendix A).

290 **Evaluation setup.** In the main results, we mainly report the grounding accuracy (%) as a metric.
 291 The prediction is counted as correct when the predicted point lies inside the ground-truth region.
 292 We evaluate ReGUIDE and baselines on SCREENSPOT (Cheng et al., 2024a), SCREENSPOT-v2
 293 (Wu et al., 2024), SCREENSPOT-PRO (Li et al., 2025), evaluation benchmarks for GUI grounding.
 294 Especially, SCREENSPOT-PRO is a more challenging construct with a high-resolution image (i.e., up
 295 to 3840×2160). The agentic evaluation setting is in Section 4.3. During evaluation, we generate a
 296 prediction via greedy decoding. Specific test-time scaling setting is described in Appendix A.3

297 **Training setup.** For the main experiment, we train ReGUIDE on Qwen-2.5-VL 3B/7B (Alibaba,
 298 2025). We utilize only a 20k subset of UGround (Gou et al., 2024) dataset, constituting approximately
 299 **0.2%** of its full set. First step of training for reasoning, we use the GRPO (DeepSeek, 2024) algorithm
 300 with two rewards, accuracy reward and $\lambda = 0.1$ weighted for formatting reward. For learning to
 301 predict consistent coordinates under transformations, where the local view is a random crop of up to
 302 30% of the original area while preserving aspect ratio. Additionally, to demonstrate that ReGUIDE
 303 can be orthogonally applied on top of diverse base models, we perform consistency fine-tuning
 304 using the same training setup with only 2k dataset samples on several publicly available checkpoints,
 305 including UI-AGILE-7B (Lian et al., 2025), and Holo1.5-7B (H-Company, 2025). These results
 306 highlight that our consistency objective improves grounding performance regardless of the underlying
 307 model architecture or pretraining data. More setups in Appendix A.3.

308 **Baselines.** We compare our method against several baselines, which fall into two categories. First,
 309 we consider the model Qwen-VL-2.5 3B/7B supervised fine-tuned (SFT) on the identical dataset
 310 with ReGUIDE (i.e., 20k UGround subset). SFT optimises a coordinate-only loss and does not
 311 generate reasoning. Additionally, we consider proprietary models and GUI grounding models: GPT-
 312 4o (OpenAI, 2024), Claude3.7 (Anthropic., 2025), SeeClick (Cheng et al., 2024b), OS-Atlas-7B (Wu
 313 et al., 2024), AGUVIS-7B (Xu et al., 2024), UGround (Gou et al., 2024), and more.

315 4.1 MAIN RESULTS

317 As shown in Table 1, we present the main result by comparing the GUI grounding performance with
 318 other baselines. Here, we mainly compare ReGUIDE with open, closed models and SFT baseline.

319 **Comparison with controlled group.** First, compare models trained with the same base architecture
 320 (Qwen-2.5-VL) and dataset (a 20k subset of UGround). Our proposed method, ReGUIDE, signifi-
 321 cantly outperforms supervised fine-tuning (SFT) baselines across all evaluated scenarios. For instance,
 322 ReGUIDE achieves an accuracy of 88.0% on SCREENSPOT with the 3B model. Similar improve-
 323 ments are observed for the more challenging SCREENSPOT-PRO benchmark, where ReGUIDE boosts

324
 325 Table 2: Accuracy (%) for other baselines and the model trained further with ReGUIDE. We
 326 evaluate on three web-grounding benchmarks: We evaluate on three web-grounding benchmarks:
 327 SCREENSPOT (ScrSpot), SCREENSPOT-v2 (ScrSpot-v2), and SCREENSPOT-PRO (ScrSpot-pro).
 328 The *Proprietary Models* include proprietary systems, while *Open-Sourced* covers public research
 329 models, The *GUI-trained + ReGUIDE* include the model trained further by ReGUIDE.

Methods	Data Size	SCRSPOT	SCRSPOT-V2	SCRSPOT-PRO
<i>Proprietary Models</i>				
GPT-4o (OpenAI, 2024)	-	18.3	16.6	0.8
Claude 3.7 (Anthropic., 2025)	-	82.1	87.6	27.7
<i>Open-Sourced</i>				
SeeClick (Cheng et al., 2024b)	1M	53.4	55.1	1.1
OS-Atlas-7B (Wu et al., 2024)	13M	82.5	84.1	18.9
AGUVIS-7B (Xu et al., 2024)	1M	84.4	85.8	22.9
Aria-UI-7B (Yang et al., 2025b)	1M	82.4	-	11.3
SE-GUI-7B (Yuan et al., 2025)	3K	88.2	90.3	47.3
GUI-G2-7B (Tang et al., 2025)	100K	92.0	93.3	47.5
GTA1-7B (Yang et al., 2025a)	70K	-	92.4	50.1
UI-Venus-7B (Gu et al., 2025)	107K	-	94.1	50.8
GUI-ARP-7B (Ye et al., 2025)	5K	89.3	91.8	60.8
<i>GUI-trained + ReGUIDE</i>				
UI-AGILE-7B (Lian et al., 2025)	9K	90.6	92.0	44.0
+ ReGUIDE (Ours)	+ 2K	92.0	92.8	50.8
Holo1.5-7B (H-Company, 2025)	-	91.7	93.9	57.8
+ ReGUIDE (Ours)	+ 2K	92.0	94.3	63.2

349
 350 performance from 23.9% to 44.5%. Also in SCREENSPOT-v2 and dataset, ReGUIDE outperforms
 351 baseline and SFT model with a meaningful margin.
 352

353 **Orthogonal adaptation on open-sourced models.** To further demonstrate the proposed consistency
 354 training and test-time scaling strategies can push existing models performance, we additionally apply
 355 ReGUIDE’s consistency training fine-tuning with only additional 2k data samples and test-time
 356 scaling to several publicly available base models, including UI-AGILE-7B, and Holo1.5-7B. As
 357 shown in Table 1, ReGUIDE consistently improves the grounding performance of these models. For
 358 example, UI-AGILE-7B improves from 44.0% to 50.8%, while Holo1.5-7B improves from 57.8% to
 359 63.2% on SCREENSPOT-PRO. Also, the adapted Holo1.5-7B achieves the best performance among
 360 all 7B-sized models (63.2%). These results shows that the components of ReGUIDE are effective
 361 on various models and ReGUIDE can serve as a orthogonal mechanism that enhances existing GUI
 362 grounding systems.

363 **Comparison with open-sourced and proprietary models.** Beyond models trained with the same
 364 data and architecture, ReGUIDE achieves competitive or superior performance against to open-
 365 sourced and proprietary models. Specifically on SCREENSPOT, our 3B model surpasses UGround-7B
 366 (88.0 % > 86.3 %) and ReGUIDE’s 7B model’s show superior results (90.2 %) against other baselines.
 367 Also, ReGUIDE consistently outperforms other baselines in SCREENSPOT-v2, too. ReGUIDE shows
 368 the most remarkable performance on SCREENSPOT-PRO. ReGUIDE-7B performs accuracy of 47.1 %,
 369 significantly outperforming UGround-7B (31.1%). We report comparison against additional baselines
 370 in Appendix B.1, which also ReGUIDE consistently outperforms baselines. **Importantly, when**
 371 **combine ReGUIDE’s training and KDE-inference scheme to other open-sourced 7B checkpoints**
 372 **such as Holo1.5-7B exhibit further gains (57.8% → 63.2%).** The combined model achieves the
 373 highest accuracy among public 7B-scale GUI grounding models, demonstrating that ReGUIDE can
 374 elevate performance of existing systems despite variations in their data.

375 **Training Efficiency of ReGUIDE.** These results demonstrate that ReGUIDE not only surpasses
 376 supervised finetuned within the same training dataset but also establishes a new competitive standard
 377 against much larger, heavily trained open and closed models. Importantly, ReGUIDE achieves these
 378 improvements *using only a small fraction of the data* (*a 20k subset of UGround*) compared to other
 379 models (i.e., UGround: 10M, AGUVIS: 1M), highlighting its data efficiency and scalability. By

378 Table 3: Grounding Accuracy (%) for ReGUIDE (Ours) and UGround on the SCREENSPOT domain
 379 split. Results are broken down by device type, and UI element type. The right-most column reports
 380 the overall average. **Bold** indicates the best result within each column.

Model	Data Size	Mobile		Desktop		Web		Average
		Text	Icon	Text	Icon	Text	Icon	
UGround-2B (Gou et al., 2024)	10M	89.4	72.0	88.7	65.7	81.3	68.9	77.7
UGround-7B (Gou et al., 2024)	10M	93.0	79.9	93.8	76.4	90.9	84.0	86.3
ReGUIDE-3B	20K	95.6	83.4	92.8	80.0	90.0	81.6	88.0
ReGUIDE-7B	20K	95.6	85.6	94.3	85.7	92.6	84.5	90.2

Table 4: Example of ReGUIDE’s generated reasoning and predicted coordinate.



Target Prompt: Choose WeChat.

Response: <think> The task is to find the coordinate of the “WeChat” app icon in the image. The image shows a section labeled “Top free apps” with icons and names of apps. The “WeChat” app icon is located in the first row, first column of this section. </think>
 <answer>(110, 437)</answer>

398 combining reinforcement learning, transform consistency learning, and scalable searching inference,
 399 ReGUIDE achieves a strong performance.

4.2 ADDITIONAL ANALYSIS AND ABLATION

404 **Generalizability over several domains.** We further analyze the generalizability of ReGUIDE across
 405 various GUI domains in multiple device environments (Mobile, Desktop, Web) and UI element types
 406 (Text, Icon). While our main results in Table 1 report the average accuracy on the SCREENSPOT, here
 407 we provide a more fine-grained evaluation. As shown in Table 3, ReGUIDE consistently achieves
 408 superior or competitive performance compared to the state-of-the-art open-sourced base model (i.e.,
 409 Uground (Gou et al., 2024)). These results indicate that the training schemes of ReGUIDE effectively
 410 enhance its ability to generalize across diverse environments. Notably, ReGUIDE particularly shows
 411 strong performance for Icon elements within the Mobile and Desktop domains.

412 **Relative spatial reasoning from generation examples.** We analyze the reasoning path generated
 413 by ReGUIDE and the associated spatial predictions. First, we observe that the model naturally
 414 decomposes GUI localization tasks into interpretable reasoning steps, referencing relative spatial
 415 information. As shown in Table 4, the model explicitly identifies intermediate visual landmarks (e.g.,
 416 a labeled section of “Top free apps”) before specifying precise coordinates based on relative positions
 417 (e.g., “first row, first column”). This structured, relative reasoning pattern supports the models’ ability
 418 to generalize across varying UI layouts.

419 **Ablation of training and inference components.** We perform an analysis on each component
 420 of ReGUIDE, specifically spatial reasoning (Reasoning), learn consistency under transformation
 421 (Consistency), and test-time searching (Searching). As shown in Table 5, each component plays an
 422 important role, leading to gradual and significant improvements when applied sequentially. Additional
 423 comparisons of alternative RL policy-optimization algorithms are provided in Appendix C.

424 **Effectiveness of Kernel Density Estimation.** To evaluate the effectiveness of Kernel Density Esti-
 425 mation (KDE) as an aggregating strategy, we con-
 426 ducted an ablation study using ReGUIDE-3B, com-
 427 paring KDE against two alternatives: *Center* and
 428 *Medoid*. *Center* computes the mean of all predicted
 429 coordinates, while *Medoid* selects the prediction
 430 that minimizes the sum of distances to all others.
 431 As shown in Table 6, KDE significantly out-
 432 performs other voting strategies. This suggests that KDE provides a more stable aggregation by
 433 down-weighting the effect of outliers.

434 Table 6: Comparison of voting algorithm on
 435 SCREENSPOT and SCREENSPOT-PRO.

Methods	SCREENSPOT	SCREENSPOT-PRO
Center	80.3	20.2
Medoid	84.6	29.4
KDE (Ours)	88.0	44.5

432 Table 5: Contribution of each proposed component of ReGUIDE on GUI grounding. We tested all
 433 three training components trained with Qwen-2.5-VL-3B: learn spatial reasoning (Reason), learn
 434 consistency under transformation (Consistency), and test-time spatial searching (Search). We report
 435 the GUI grounding accuracy (%) on SCREENSPOT and SCREENSPOT-PRO benchmarks.

Model Size	Reason	Consistency	Search	SCREENSPOT	SCREENSPOT-PRO
3B	✗	✗	✗	55.5	23.9
	✓	✗	✗	83.3	27.2
	✓	✓	✗	84.9	27.9
	✓	✗	✓	85.2	40.7
	✓	✓	✓	88.0	44.5

442 Table 7: Contribution of each proposed component for test-time scaling, namely, the cropping and
 443 voting. We report the grounding accuracy (%) on SCREENSPOT and SCREENSPOT-PRO benchmarks
 444 with ReGUIDE-3B. The bold indicates the best results.

Cropping	Voting	SCREENSPOT	SCREENSPOT-PRO
✗	✗	84.3	27.9
✓	✗	81.7	42.7
✓	✓	88.0	44.5

450 **Ablation of inference components.** Moreover, we perform ablation to prove the effectiveness of
 451 each component in the two-stage inference time searching strategy. As shown in Table 7, both the
 452 crop stage and the voting stage contribute to improvement in performance. It is notable that in
 453 SCREENSPOT-PRO, the improvement induced by crop stage is huge, which indicates that localization
 454 plays a crucial role for the proper understanding of high-resolution images.

455 **Internal attention after consistency finetuning.** To as-
 456 sess how the consistency-under-transformation stage alters
 457 internal representations, we visualised the average atten-
 458 tion logits of the last transformer layer in ReGUIDE-3B.
 459 As shown in Figure 2, the GRPO-only concentrates most
 460 of its attention on the reasoning span, which indicates
 461 limited contextual grounding. In contrast, the ReGUIDE
 462 model, after consistency finetuning, distributes attention
 463 more evenly across reasoning and other text tokens. This
 464 result imply that consistency finetuning enables richer spa-
 465 tial awareness and reduced attention collapse.

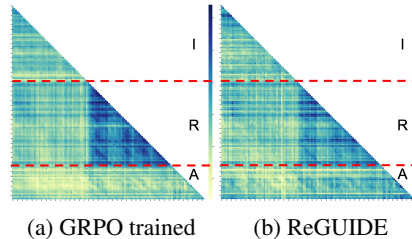


Figure 2: Attention map of text tokens. *I*: instruction, *R*: rationale, and *A*: answer.

466 Natural Gaussian distribution of coordinate tokens likelihood.

467 As an additional qualitative analysis, we examine the likelihood
 468 distribution of coordinates in the neighborhood of the initial pre-
 469 dicted point, conditioned on the same generated reasoning. As
 470 shown in Figure 3, theses likelihoods form a surprisingly smooth,
 471 Gaussian-shaped distribution. This Gaussian pattern suggests that
 472 the ReGUIDE implicitly captures continuous spatial uncertainty,
 473 despite operating in discrete language token space. The observation
 474 provides a strong empirical motivation for our proposed Gaussian-
 475 weighted inference strategy (i.e., KDE), which leverages them to
 476 improve coordinate prediction accuracy and robustness. [Seemingly, a concurrent work GUI-G2](#) (Tang et al., 2025) also suggested a
 477 Gaussian-shaped structure, but in a fundamentally difference purpose: [GUI-G2 introduces a Gaussian](#)
 478 [reward during training, inspired from findings in human cursor control research \(Fitts, 1954\).](#) How-
 479 [ever, ReGUIDE leverages the Gaussian structure explicitly at test-time through our scaling procedure](#)
 480 [rather than using it for training. Notably, our empirical observation not only supports the design](#)
 481 [choice of our KDE-based inference, but also suggests a potential explanation for why Gaussian-based](#)
 482 [reward shaping, as used in GUI-G2, may be inherently effective.](#)

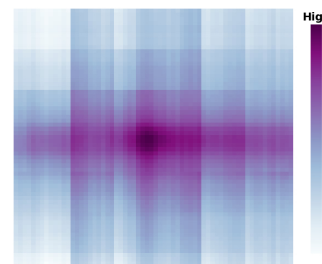


Figure 3: Likelihood of coordinate language tokens.

483 **Ablation on inference time searching strategy.** We perform ablation for three hyperparameters on
 484 inference time scaling strategy, that is, crop size (W_{ROI}), generation samples (N), and temperature (T).
 485 As shown in Figure 4, increasing N gradually improves the grounding performance, demonstrating
 that our strategy is scalable. We adopt the default hyperparameters $N = 16$, $L = 840$, and $T = 1.0$.

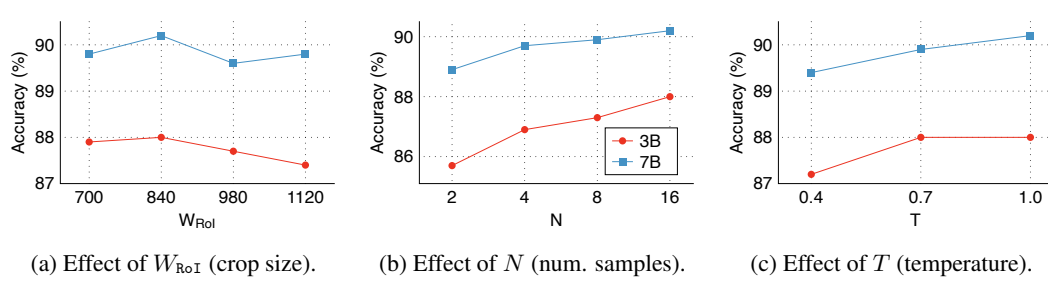
Figure 4: Ablation studies on crop size W_{RoI} , number of samples N , and decoding temperature T .

Table 8: Task-success rate (%) on the two offline-agent task benchmarks, i.e., Multimodal-Mind2Web (MM2W), and Android Control (AC). For Multimodal-Mind2Web, there are 3 test sets cross-domain, cross-task, and cross-web. For Android Control, there are 2 test sets low and high.

Grounding Module	Data Size	MM2W			AC	
		domain	task	web	low	high
UGround-2B (Gou et al., 2024)	10M	47.7	48.6	47.6	65.0	50.0
UGround-7B (Gou et al., 2024)	10M	48.5	50.7	48.1	66.2	49.8
ReGUIDE-3B (Ours)	20K	48.8	50.5	47.7	66.2	49.8
ReGUIDE-7B (Ours)	20K	49.5	52.0	48.7	67.4	50.0

4.3 AGENTIC SETTINGS EXPERIMENTS

To verify whether better grounding transfers to real tasks, we plug each grounding model with ReGUIDE and use a high-level planner (GPT-4o). For every episode, the planner emits a natural-language action plan; the grounding module converts each step into pixel coordinates. Here, we report task-success rate (%) on five offline suites: Multimodal-Mind2Web (Deng et al., 2023), AndroidControl (Li et al., 2024). All prompts, settings, and frameworks are followed by UGround (Gou et al., 2024) and the detailed settings are described in Appendix A.

As shown in Table 8, improved grounding performance made by ReGUIDE leads to better agent performance. With only 3B parameters, ReGUIDE matches or edges out the larger UGround-7B on Multimodal-Mind2Web and Android Control-High. The 7B variant of ReGUIDE consistently outperforms other baselines (i.e., +1.3% in Multimodal-Mind2Web cross task). These gains, achieved with identical planners and action budgets, substantiate that the grounding improvements provided by self-evolutionary RL and global-local consistency directly enhance full-task completion.

5 DISCUSSION AND CONCLUSION

We proposed ReGUIDE, a novel and effective GUI grounding framework that significantly enhances the capabilities of Multimodal Large Language Models by enabling data-efficient learning through self-generated reasoning and spatial-aware criticism. Our key idea is leveraging online reinforcement learning for self-generating language reasoning and employing spatial priors to criticize predictions, and further boosting performance at inference time through a test-time scaling search strategy that integrates spatial search with coordinate aggregation. We demonstrated that ReGUIDE consistently outperforms other open-sourced baselines, even when trained with a tiny fraction of data, such as only 0.2% of the samples used by the best open-sourced baselines. Crucially, these advances in data-efficient grounding translate to improved performance in downstream agentic tasks, highlighting ReGUIDE’s potential to develop more capable and practical GUI agents.

Future works and limitations. We believe it will be an interesting future direction to train MLLM planners that can operate hierarchically with ReGUIDE, fully capitalizing on its precise grounding performance. Additionally, a potential limitation is that while ReGUIDE is a very effective method, it lacks an explicit safety framework to prevent malicious uses, such as hacking or spreading misinformation—a challenge common to many grounding models. However, future investigations could explore the research and development of robust safeguards.

540 ETHICS STATEMENT
541

542 This paper presents ReGUIDE, a method that significantly improves GUI-grounding accuracy. We
543 expect that our approach will enhance digital accessibility and productivity by enabling agents to
544 locate and interact with on-screen elements more reliably. However, the same capability could be
545 misused for malicious purposes, such as automated hacking or spreading misinformation, issues that
546 current agent models already face. Mitigation measures include responsible release practices, access
547 controls, and detection tools to discourage adversarial deployments.

548
549 REPRODUCIBILITY STATEMENT
550

551 We have made extensive efforts to ensure the reproducibility of our results. Conceptual and ex-
552 perimental details are provided in Section 4, including dataset descriptions and evaluation setups.
553 Training configurations, optimization hyperparameters, and evaluation protocols are described in
554 Appendix A.3, while details of the computational resources used are summarized in Appendix A.4.
555 To further facilitate reproducibility, we provide our implementation and scripts in the supple-
556 mentary materials, which include the codebase for training, evaluation, and inference. Together, these
557 resources should allow researchers to reproduce our experiments and follow the reported results.

558
559 REFERENCES
560

561 Arash Ahmadian, Chris Cremer, Matthias Gallé, Marzieh Fadaee, Julia Kreutzer, Olivier Pietquin,
562 Ahmet Üstün, and Sara Hooker. Back to basics: Revisiting reinforce style optimization for learning
563 from human feedback in llms. *arXiv preprint arXiv:2402.14740*, 2024.

564 Alibaba. Qwen2.5-vl technical report. *arXiv preprint arXiv:abs/2502.13923*, 2025.

566 Team Anthropic. Introducing computer use, a new claudie 3.5 sonnet, and claudie 3.5 haiku. <https://www.anthropic.com/news/3-5-models-and-computer-use>, October 2024.

569 Team Anthropic. Claude 3.7 sonnet and claudie code. <https://www.anthropic.com/news/claude-3-7-sonnet>, February 2025.

571 Mathilde Caron, Hugo Touvron, Ishan Misra, Hervé Jégou, Julien Mairal, Piotr Bojanowski, and
572 Armand Joulin. Emerging properties in self-supervised vision transformers. In *Proceedings of the*
573 *IEEE/CVF international conference on computer vision*, pp. 9650–9660, 2021.

575 Chaoran Chen, Zhiping Zhang, Ibrahim Khalilov, Bingcan Guo, Simret A Gebreegziabher, Yanfang
576 Ye, Ziang Xiao, Yaxing Yao, Tianshi Li, and Toby Jia-Jun Li. Toward a human-centered evaluation
577 framework for trustworthy llm-powered gui agents. *arXiv preprint arXiv:2504.17934*, 2025.

578 Kanzhi Cheng, Qiushi Sun, Yougang Chu, Fangzhi Xu, Yantao Li, Jianbing Zhang, and Zhiy-
579 ong Wu. Seeclick: Harnessing gui grounding for advanced visual gui agents. *arXiv preprint*
580 *arXiv:2401.10935*, 2024a.

582 Kanzhi Cheng, Qiushi Sun, Yougang Chu, Fangzhi Xu, Yantao Li, Jianbing Zhang, and Zhiy-
583 ong Wu. Seeclick: Harnessing gui grounding for advanced visual gui agents. *arXiv preprint*
584 *arXiv:2401.10935*, 2024b.

585 Team DeepSeek. Deepseekmath: Pushing the limits of mathematical reasoning in open language
586 models. *arXiv preprint arXiv:2402.03300*, 2024.

588 Xiang Deng, Yu Gu, Boyuan Zheng, Shijie Chen, Samuel Stevens, Boshi Wang, Huan Sun, and
589 Yu Su. Mind2web: Towards a generalist agent for the web. In *Thirty-seventh Conference on*
590 *Neural Information Processing Systems*, 2023. URL <https://openreview.net/forum?id=kiYqbO3wqw>.

592 Paul M Fitts. The information capacity of the human motor system in controlling the amplitude of
593 movement. *Journal of experimental psychology*, 47(6):381, 1954.

594 Boyu Gou, Ruohan Wang, Boyuan Zheng, Yanan Xie, Cheng Chang, Yiheng Shu, Huan Sun, and
 595 Yu Su. Navigating the digital world as humans do: Universal visual grounding for gui agents.
 596 *arXiv preprint arXiv:2410.05243*, 2024.

597

598 Zhangxuan Gu, Zhengwen Zeng, Zhenyu Xu, Xingran Zhou, Shuheng Shen, Yunfei Liu, Beiting
 599 Zhou, Changhua Meng, Tianyu Xia, Weizhi Chen, et al. Ui-venus technical report: Building
 600 high-performance ui agents with rft. *arXiv preprint arXiv:2508.10833*, 2025.

601 Daya Guo, Dejian Yang, Haowei Zhang, Junxiao Song, Ruoyu Zhang, Runxin Xu, Qihao Zhu,
 602 Shirong Ma, Peiyi Wang, Xiao Bi, et al. Deepseek-r1: Incentivizing reasoning capability in llms
 603 via reinforcement learning. *arXiv preprint arXiv:2501.12948*, 2025.

604

605 H-Company. Holo1.5 - open foundation models for computer use agents,
 606 2025. URL <https://huggingface.co/collections/Hcompany/holo15-68c1a5736e8583a309d23d9b>.

607

608 R Devon Hjelm, Alex Fedorov, Samuel Lavoie-Marchildon, Karan Grewal, Phil Bachman, Adam
 609 Trischler, and Yoshua Bengio. Learning deep representations by mutual information estimation
 610 and maximization. *arXiv preprint arXiv:1808.06670*, 2018.

611

612 Wenyi Hong, Weihan Wang, Qingsong Lv, Jiazheng Xu, Wenmeng Yu, Junhui Ji, Yan Wang, Zihan
 613 Wang, Yuxiao Dong, Ming Ding, et al. Cogagent: A visual language model for gui agents.
 614 In *Proceedings of the IEEE/CVF Conference on Computer Vision and Pattern Recognition*, pp.
 14281–14290, 2024.

615

616 Arian Hosseini, Xingdi Yuan, Nikolay Malkin, Aaron Courville, Alessandro Sordoni, and Rishabh
 617 Agarwal. V-star: Training verifiers for self-taught reasoners. *arXiv preprint arXiv:2402.06457*,
 618 2024.

619

620 Jian Hu. Reinforce++: A simple and efficient approach for aligning large language models. *arXiv
 preprint arXiv:2501.03262*, 2025.

621

622 Wenxuan Huang, Bohan Jia, Zijie Zhai, Shaosheng Cao, Zheyu Ye, Fei Zhao, Zhe Xu, Yao Hu, and
 623 Shaohui Lin. Vision-r1: Incentivizing reasoning capability in multimodal large language models.
 624 *arXiv preprint arXiv:2503.06749*, 2025.

625

626 Woosuk Kwon, Zhuohan Li, Siyuan Zhuang, Ying Sheng, Lianmin Zheng, Cody Hao Yu, Joseph E.
 627 Gonzalez, Hao Zhang, and Ion Stoica. Efficient memory management for large language model
 628 serving with pagedattention. In *Proceedings of the ACM SIGOPS 29th Symposium on Operating
 Systems Principles*, 2023.

629

630 Andrew K Lampinen, Ishita Dasgupta, Stephanie CY Chan, Kory Mathewson, Michael Henry
 631 Tessler, Antonia Creswell, James L McClelland, Jane X Wang, and Felix Hill. Can language
 632 models learn from explanations in context? *arXiv preprint arXiv:2204.02329*, 2022.

633

634 Hyunseok Lee, Seunghyuk Oh, Jaehyung Kim, Jinwoo Shin, and Jihoon Tack. Revise: Learning to
 refine at test-time via intrinsic self-verification. *arXiv preprint arXiv:2502.14565*, 2025.

635

636 Kaixin Li, Ziyang Meng, Hongzhan Lin, Ziyang Luo, Yuchen Tian, Jing Ma, Zhiyong Huang, and
 637 Tat-Seng Chua. Screenspot-pro: Gui grounding for professional high-resolution computer use.
 638 *arXiv preprint arXiv:2504.07981*, 2025.

639

640 Wei Li, William Bishop, Alice Li, Chris Rawles, Folawiyo Campbell-Ajala, Divya Tyamagundlu,
 641 and Oriana Riva. On the effects of data scale on computer control agents. *arXiv preprint
 arXiv:2406.03679*, 2024.

642

643 Shuquan Lian, Yuhang Wu, Jia Ma, Yifan Ding, Zihan Song, Bingqi Chen, Xiawu Zheng, and Hui Li.
 644 Ui-agile: Advancing gui agents with effective reinforcement learning and precise inference-time
 645 grounding. *arXiv preprint arXiv:2507.22025*, 2025.

646

647 Kevin Qinghong Lin, Linjie Li, Difei Gao, Zhengyuan Yang, Shiwei Wu, Zechen Bai, Weixian Lei,
 648 Lijuan Wang, and Mike Zheng Shou. Showui: One vision-language-action model for gui visual
 649 agent. *arXiv preprint arXiv:2411.17465*, 2024.

648 Zhengxi Lu, Yuxiang Chai, Yaxuan Guo, Xi Yin, Liang Liu, Hao Wang, Guanjing Xiong, and
 649 Hongsheng Li. Ui-r1: Enhancing action prediction of gui agents by reinforcement learning. *arXiv*
 650 *preprint arXiv:2503.21620*, 2025.

651 Tiange Luo, Lajanugen Logeswaran, Justin Johnson, and Honglak Lee. Visual test-time scaling for
 652 gui agent grounding. *arXiv preprint arXiv:2505.00684*, 2025.

653 Xinyu Ma, Ziyang Ding, Zhicong Luo, Chi Chen, Zonghao Guo, Derek F Wong, Xiaoyi Feng,
 654 and Maosong Sun. Deepperception: Advancing r1-like cognitive visual perception in mllms for
 655 knowledge-intensive visual grounding. *arXiv preprint arXiv:2503.12797*, 2025.

656 Maxwell Nye, Anders Johan Andreassen, Guy Gur-Ari, Henryk Michalewski, Jacob Austin, David
 657 Bieber, David Dohan, Aitor Lewkowycz, Maarten Bosma, David Luan, et al. Show your work:
 658 Scratchpads for intermediate computation with language models. *arXiv preprint arXiv:2112.00114*,
 659 2021.

660 OpenAI. Gpt-4o system card. *arXiv preprint arXiv:2410.21276*, 2024.

661 Maxime Oquab, Timothée Darcet, Théo Moutakanni, Huy Vo, Marc Szafraniec, Vasil Khalidov,
 662 Pierre Fernandez, Daniel Haziza, Francisco Massa, Alaaeldin El-Nouby, et al. Dinov2: Learning
 663 robust visual features without supervision. *arXiv preprint arXiv:2304.07193*, 2023.

664 Yujia Qin, Yining Ye, Junjie Fang, Haoming Wang, Shihao Liang, Shizuo Tian, Junda Zhang, Jiahao
 665 Li, Yunxin Li, Shijue Huang, et al. Ui-tars: Pioneering automated gui interaction with native
 666 agents. *arXiv preprint arXiv:2501.12326*, 2025.

667 Christopher Rawles, Sarah Clinckemaillie, Yifan Chang, Jonathan Waltz, Gabrielle Lau, Marybeth
 668 Fair, Alice Li, William Bishop, Wei Li, Folawiyo Campbell-Ajala, Daniel Toyama, Robert Berry,
 669 Divya Tyamagundlu, Timothy Lillicrap, and Oriana Riva. Androidworld: A dynamic benchmarking
 670 environment for autonomous agents, 2024. URL <https://arxiv.org/abs/2405.14573>.

671 Steven J Rennie, Etienne Marcheret, Youssef Mroueh, Jerret Ross, and Vaibhava Goel. Self-critical
 672 sequence training for image captioning. In *IEEE Conference on Computer Vision and Pattern
 673 Recognition*, pp. 7008–7024, 2017.

674 M Rosenblat. Remarks on some nonparametric estimates of a density function. *Ann. Math. Stat.* 27:
 675 832–837, 1956.

676 Peter Shaw, Mandar Joshi, James Cohan, Jonathan Berant, Panupong Pasupat, Hexiang Hu, Urvashi
 677 Khandelwal, Kenton Lee, and Kristina N Toutanova. From pixels to ui actions: Learning to follow
 678 instructions via graphical user interfaces. *Advances in Neural Information Processing Systems*, 36:
 679 34354–34370, 2023.

680 Charlie Snell, Jaehoon Lee, Kelvin Xu, and Aviral Kumar. Scaling llm test-time compute optimally
 681 can be more effective than scaling model parameters. *arXiv preprint arXiv:2408.03314*, 2024.

682 Fei Tang, Zhangxuan Gu, Zhengxi Lu, Xuyang Liu, Shuheng Shen, Changhua Meng, Wen Wang,
 683 Wenqi Zhang, Yongliang Shen, Weiming Lu, et al. Gui-g2: Gaussian reward modeling for gui
 684 grounding. *arXiv preprint arXiv:2507.15846*, 2025.

685 Shuai Wang, Weiwen Liu, Jingxuan Chen, Yuqi Zhou, Weinan Gan, Xingshan Zeng, Yuhan Che,
 686 Shuai Yu, Xinlong Hao, Kun Shao, et al. Gui agents with foundation models: A comprehensive
 687 survey. *arXiv preprint arXiv:2411.04890*, 2024.

688 Penghao Wu and Saining Xie. V*: Guided visual search as a core mechanism in multimodal llms.
 689 In *Proceedings of the IEEE/CVF Conference on Computer Vision and Pattern Recognition*, pp.
 690 13084–13094, 2024.

691 Zhiyong Wu, Zhenyu Wu, Fangzhi Xu, Yian Wang, Qiushi Sun, Chengyou Jia, Kanzhi Cheng, Zichen
 692 Ding, Liheng Chen, Paul Pu Liang, et al. Os-atlas: A foundation action model for generalist gui
 693 agents. *arXiv preprint arXiv:2410.23218*, 2024.

694 Xiaobo Xia and Run Luo. Gui-r1: A generalist r1-style vision-language action model for gui agents.
 695 *arXiv preprint arXiv:2504.10458*, 2025.

702 Yiheng Xu, Zekun Wang, Junli Wang, Dunjie Lu, Tianbao Xie, Amrita Saha, Doyen Sahoo, Tao Yu,
 703 and Caiming Xiong. Aguvis: Unified pure vision agents for autonomous gui interaction. *arXiv*
 704 *preprint arXiv:2412.04454*, 2024.

705 Yan Yang, Dongxu Li, Yutong Dai, Yuhao Yang, Ziyang Luo, Zirui Zhao, Zhiyuan Hu, Junzhe
 706 Huang, Amrita Saha, Zeyuan Chen, et al. Gta1: Gui test-time scaling agent. *arXiv preprint*
 707 *arXiv:2507.05791*, 2025a.

708 Yuhan Yang, Yue Wang, Dongxu Li, Ziyang Luo, Bei Chen, Chao Huang, and Junnan Li. Aria-ui:
 709 Visual grounding for gui instructions. In *Findings of the Association for Computational Linguistics: ACL 2025*, pp. 22418–22433, 2025b.

710 Xianhang Ye, Yiqing Li, Wei Dai, Miancan Liu, Ziyuan Chen, Zhangye Han, Hongbo Min, Jinkui
 711 Ren, Xiantao Zhang, Wen Yang, et al. Gui-arp: Enhancing grounding with adaptive region
 712 perception for gui agents. *arXiv preprint arXiv:2509.15532*, 2025.

713 Tianyu Yu, Yuan Yao, Haoye Zhang, Taiwen He, Yifeng Han, Ganqu Cui, Jinyi Hu, Zhiyuan Liu,
 714 Hai-Tao Zheng, Maosong Sun, et al. Rlhf-v: Towards trustworthy mllms via behavior alignment
 715 from fine-grained correctional human feedback. In *Proceedings of the IEEE/CVF Conference on
 Computer Vision and Pattern Recognition*, pp. 13807–13816, 2024.

716 Xinbin Yuan, Jian Zhang, Kaixin Li, Zhuoxuan Cai, Lujian Yao, Jie Chen, Enguang Wang, Qibin Hou,
 717 Jinwei Chen, Peng-Tao Jiang, et al. Enhancing visual grounding for gui agents via self-evolutionary
 718 reinforcement learning. *arXiv preprint arXiv:2505.12370*, 2025.

719 Junlei Zhang, Zichen Ding, Chang Ma, Zijie Chen, Qiushi Sun, Zhenzhong Lan, and Junxian
 720 He. Breaking the data barrier–building gui agents through task generalization. *arXiv preprint*
 721 *arXiv:2504.10127*, 2025.

722 Haoren Zhao, Tianyi Chen, and Zhen Wang. On the robustness of gui grounding models against
 723 image attacks. *arXiv preprint arXiv:2504.04716*, 2025.

724 Yao Zhao, Zhitian Xie, Chen Liang, Chenyi Zhuang, and Jinjie Gu. Lookahead: An inference
 725 acceleration framework for large language model with lossless generation accuracy. In *Proceedings*
 726 *of the 30th ACM SIGKDD Conference on Knowledge Discovery and Data Mining*, pp. 6344–6355,
 727 2024.

728 Boyuan Zheng, Boyu Gou, Jihyung Kil, Huan Sun, and Yu Su. Gpt-4v(ision) is a generalist web
 729 agent, if grounded. In *Forty-first International Conference on Machine Learning*, 2024. URL
 730 <https://openreview.net/forum?id=piEcKJ2D1B>.

731

732

733

734

735

736

737

738

739

740

741

742

743

744

745

746

747

748

749

750

751

752

753

754

755

756

A EXPERIMENTAL DETAILS

757
758 In this section, we describe the experimental details of Section 4, including ReGUIDE and baselines.
759760

A.1 DATASET DETAILS

762 In this section, we describe the dataset we used in training and evaluation.
763

- **UGround** Uground is a Graphical User Interface (GUI) grounding dataset that consists of 10M triplets of GUI image, element coordinates, and description of the element, which was synthesized by open MLLM, Llava-Next-13 B. Uground (Gou et al., 2024) models are trained with their own synthesized web GUI dataset, which consists of 10 M image-instruction pairs. For training ReGUIDE, we randomly select a 20K image-instruction set from UGround (Gou et al., 2024) dataset, which is approximately 0.2% of the original dataset.
- **SCREENSPOT** ScreenSpot (Cheng et al., 2024a) is an evaluation benchmark dataset which consists of 1,272 (image, description, bounding box) triplets. There are various GUI domains in multiple device environments (Mobile, Desktop, Web) and UI element types (Text, Icon).
- **SCREENSPOT-V2** Wu et al. (2024) refined the original ScreenSpot dataset by resolving ambiguous descriptions and aligning annotations more precisely with visual elements. We use both versions for a more accurate grounding evaluation.
- **SCREENSPOT-PRO** ScreenSpot-Pro (Li et al., 2025) is a benchmark designed to evaluate GUI grounding models in professional, high-resolution environments. It spans 23 applications across five professional categories and three operating systems, highlighting the challenges models face when interacting with complex software..
- **Android Control** Android Control (Li et al., 2024) is an offline agent benchmark comprising 15000 distinct user tasks sampled from 833 different Android applications. Each task contains a sequence of screenshots, detailed action records, and accessibility trees derived from human demonstrations (the “golden trajectory”). Each action is also annotated with a specific instruction (e.g., “set the hours to 6”), allowing both high-level and low-level task settings. In our experiments, we followed Gou et al. (2024) and evaluated models on 500 randomly sampled steps from the test split.
- **Multimodal-Mind2Web** The Multimodal-Mind2Web (Deng et al., 2023) dataset contains screenshots with a large vertical dimension (e.g., 1280 x 10000 pixels). The test split includes 1,013 realistic user tasks collected from over 100 different websites, each accompanied by a high-level instruction and a sequence of action steps. To make the data manageable we followed (Gou et al., 2024), and divide the image vertically with certain amount of duplication. During the agent evaluation, when an agent cannot find an actionable element or explicitly chooses to scroll, the next block is processed, simulating user scrolling.

795

A.2 MODEL DETAILS

- **Qwen-2.5-VL** We use Qwen-2.5-VL (Alibaba, 2025) is a multimodal large language model (mllm) which inputs text and images and outputs text. The model is equipped with vision-language fusion modules and trained on diverse visual instruction datasets. We trained ReGUIDE from Qwen-2.5-VL-3B and 7B models.
- **UGround** UGround (Gou et al., 2024) is the model trained from Qwen-2-VL (Alibaba, 2025), there are two versions UGround-2B and UGround-7B. They are trained with a synthesized dataset that has 10M images, instructions, and target coordinates triplets. This amount of dataset size is about 500 times bigger than the ReGUIDE trained. For the fair comparison, we trained UGround on Qwen-2.5-VL (Alibaba, 2025) with the same subset used to train ReGUIDE. As shown in Table 1, ReGUIDE excessively outperforms UGround for both.
- **Proprietary Models Endpoint**
 - *gpt-4o-2024-05-13*
 - *claude-3-7-sonnet-20250219*

810 A.3 TRAINING AND EVALUATION DETAILS
811

812 • **Training framework** For the training framework, we utilize VERL for reinforcement learning
813 and TRL for fine-tuning.

814 – TRL (<https://github.com/huggingface/trl>)
815 – VERL (<https://github.com/volcengine/verl>)

816 • **Training hyperparameters.** We describe our training hyperparameters, which we used for
817 training, especially for learning to explaining GUI images via reasoning and learning to predict
818 consistent coordinates under transformations.

820 Table 9: Hyperparameters for ReGUIDE on grp training
821

823 Hyperparameter	824 Value
824 Optimizer	Adam
825 Algorithm	GRPO
826 Learning rate	1e-6
827 Training data size	20k
828 Batch size	128
829 Generation per Sample	8
830 kl_coef	0.01

831 Table 10: Hyperparameters for ReGUIDE on training consistent coordinated under transformations
832

834 Hyperparameter	835 Value
836 Optimizer	Adam
837 Learning rate	1e-6
838 Training data size	20k
839 Epoch	1
840 Batch size	64
841 minimum crop ratio	0.3

842 A.4 COMPUTE RESOURCE
843

844 For the main development, we mainly use Intel(R) Xeon(R) Gold 6338 CPU @ 2.00GHz and four
845 A100 80GB GPUs. For training ReGUIDE, it took around 20 hours.
846

847 A.5 TEST-TIME SCALING STRATEGY SETTING
848

849 For the test-time scaling strategy, if there is further mention about hyperparameter, we used prediction
850 sampling $N = M = 16$ samples with temperature $T = 1.0$, crop bounding box size as $W_{\text{RoI}} =$
851 $H_{\text{RoI}} = 840$, and KDE variance $\Sigma = 0.01$.

852
853
854
855
856
857
858
859
860
861
862
863

864 **B ADDITIONAL EXPERIMENTAL RESULTS**
865866 **B.1 COMPARISON WITH ADDITIONAL BASELINES**
867868 Table 11: Accuracy (%) for ReGUIDE (Ours) and other baselines, including UI-TARS, UI-R1,
869 GUI-R1, and ReGUIDE (Ours). We evaluate on three web-grounding benchmarks: SCREENSPOT,
870 SCREENSPOT-v2, and SCREENSPOT-PRO.
871

Methods	SCREENSPOT	SCREENSPOT-V2	SCREENSPOT-PRO	Average
UI-R1-E-3B	89.2	89.5	33.5	70.7
GUI-R1-7B	-	-	31.3	-
UI-TARS-2B	82.3	84.7	27.7	64.9
UI-TARS-7B	89.5	91.6	35.7	72.3
Qwen2.5-VL-7B + <i>Region Focus</i>	-	-	32.1	-
UI-TARS-7B + <i>Region Focus</i>	-	-	41.2	-
ReGUIDE-3B (Ours)	88.0	90.0	44.5	74.2
ReGUIDE-7B (Ours)	90.2	92.3	47.1	76.5

881 We compare the grounding accuracy of ReGUIDE with other additional baselines, which are closed-
882 source (UI-TARS (Qin et al., 2025)) and the concurrently proposed reinforcement learning methods
883 for grounding UI-R1 (Lu et al., 2025) and GUI-R1 (Xia & Luo, 2025). As shown in Table 11
884 ReGUIDE achieves the highest average combined accuracy (75.3%) across SCREENSPOT (Cheng
885 et al., 2024a), SCREENSPOT-V2 (Wu et al., 2024), and SCREENSPOT-PRO (Li et al., 2025).

886 Crucially, the compact ReGUIDE-3B already surpasses the best 7B-parameter base model (UI-TARS-
887 7B) by +1.8 pp in average accuracy (72.3 % → 74.1 %), demonstrating that our training and search
888 strategy substantially improves the GUI grounding performance. Moreover, both reinforcement
889 fine-tuned baselines (i.e., UI-R1-E-3B, GUI-R1-7B) perform worse than ReGUIDE, underscoring
890 the effectiveness of our further training for consistency under transformation and search algorithm.
891 The full-sized ReGUIDE-7B further extends this lead to +4.2 pp, establishing a best among the given
892 baselines on the combined benchmarks.

893 Moreover, we also compare ReGUIDE with the recent visual test-time scaling method, Region
894 Focus (Luo et al., 2025), which improves grounding by repeatedly focusing on local regions and
895 re-predicting actions. In contrast, ReGUIDE adopts a different approach based on cropping and
896 aggregating predictions. As analyzed in Table 6, we systematically evaluated several statistical
897 aggregation strategies and found that Kernel Density Estimation (KDE) yields the most reliable
898 results. This choice is further motivated by the Gaussian-shaped likelihood distribution observed in
899 Figure 3, which provides a natural justification for KDE as an aggregation method. Despite using
900 a smaller backbone, ReGUIDE-3B consistently outperforms Region Focus even against their 7B
901 models, highlighting both the effectiveness and efficiency of our approach.

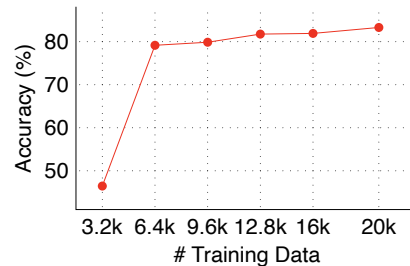
902 **B.2 EFFECT OF CONSISTENCY FINETUNING AFTER REINFORCEMENT STAGE**
903904 Table 12: Effect of consistency-under-transformation finetuning on ReGUIDE-3B, evaluated on the
905 SCREENSPOT (Cheng et al., 2024a) benchmark.
906

Method	Augmentation usage	Accuracy (%)
RL w/o Aug.	-	83.3
RL w/ Aug.	In RL stage	83.2
ReGUIDE (Ours).	fine-tune	84.9

913 We assess the benefit of our *consistency-under-transformation* finetuning on the ReGUIDE-3B model
914 using the ScreenSpot benchmark. As shown in Table 12, training GRPO on the original screenshots
915 only (RL w/o Aug.) achieves 83.3 % accuracy, while mixing the same augmented views directly into
916 the RL phase (RL w/ Aug) yields no improvement (83.2 %). In contrast, our two-stage pipeline—first
917 training GRPO without augmentation and then applying a separate consistency finetune on the
918 augmented views (ReGUIDE)—raises accuracy to 84.9 %, a gain of +1.6 pp over the vanilla RL

918 model and +1.7 pp over RL w/ Aug. This result confirms that the performance boost arises from
 919 explicitly learning to align predictions across transformed views, not from data augmentation alone.
 920

921 B.3 DATASET SCALABLE EXPERIMENT



933 Figure 5: Grounding accuracy (%) on SCREENSPOT (Cheng et al., 2024a) as the UGround (Gou
 934 et al., 2024) training set grows from 3.2 K to 20 K samples. We trained from Qwen-2.5-VL-3B.
 935

936 To measure how our reinforcement-learning stage benefits from more data, we varied the amount of
 937 UGround (Gou et al., 2024) training samples from 3.2K up to 20K in 3.2K increments and evaluated
 938 grounding accuracy (%) on the SCREENSPOT (Cheng et al., 2024a) benchmark (Figure 5). Accuracy
 939 rises monotonically with data size, and the full 20K subset yields the best performance. These results
 940 indicate that the ReGUIDE training pipeline scales effectively with additional data and has not yet
 941 saturated at the 20K level.

943 B.4 ONLINE AGENT EVALUATION

946 Table 13: Task success rate (%) on Android World.

947 Methods	948 Android World
949 UGround-7B	44.0
950 ReGUIDE-3B	46.1

952 We further evaluate ReGUIDE on the Android World (Rawles et al., 2024) online agent benchmark,
 953 comparing the grounding accuracy (%) of ReGUIDE-3B with UGround-7B (Gou et al., 2024). As
 954 shown in Table 13, ReGUIDE-3B surpasses UGround-7B by +2.1%, despite having considerably
 955 fewer parameters. This finding indicates that stronger grounding performance directly translates into
 956 improved results on complex online agent evaluations.

958 B.5 KDE-BASED TEST-TIME SCALING.

961 Table 14: Accuracy (%) for baselines including UGround-7B and GTA1-7B with KDE test-time
 962 scaling. We evaluate on two web-grounding benchmarks: SCREENSPOT-V2, and SCREENSPOT-PRO.

964 Methods	965 SCREENSPOT-V2	966 SCREENSPOT-PRO
965 UGround-7B	89.6	40.3
966 + KDE-TTS	91.0	46.6

968 We additionally evaluate the proposed KDE-based test-time scaling on several opensource base model
 969 to measure its standalone effectiveness. As shown in the Table 14, KDE-base scaling consistently
 970 improves the grounding accuracy of the model (i.e., UGround-7B) across both ScreenSpot-v2 and
 971 ScreenSpot-pro. For example, UGround -7B improves from 40.4% to 46.6% on SCREENSPOT-PRO.
 972 These results confirm that KDE-based search works as a model-agnostic inference enhancement.

972 Table 15: Comparison of the average consuming prediction time and grounding accuracy (%) on
 973 SCREENSPOT and SCREENSPOT-PRO benchmarks with ReGUIDE-3B. **N** denotes the number of
 974 sampling during test-time.

975 976 977 978 979 980 981 982 983 984 985 986 987 988 989 990 991 992 993 994 995 996 997 998 999 1000 1001 1002 1003 1004 1005 1006 1007 1008 1009 1010 1011 1012 1013 1014 1015 1016 1017 1018 1019 1020 1021 1022 1023 1024 1025	Method	Scaling	N	SCREENSPOT			SCREENSPOT-PRO		
				Time (s)	Time Cost	Accuracy	Time (s)	Time Cost	Accuracy
ReGUIDE-3B	✗	-	1.69	x1.0	84.9	2.43	x1.0	27.9	
	✓	4	3.06	x1.8	86.9	3.98	x1.6	41.1	
	✓	8	3.31	x2.0	87.3	4.29	x1.8	43.5	
	✓	16	3.76	x2.2	88.0	4.88	x2.0	44.5	

B.6 COMPUTATION COST OF THE INFERENCE

We measured the average elapsed time for inference of samples in ReGUIDE and compared between with and without test-time inference procedure. We used a single A100 80G GPU for fair comparison, and employed the vLLM (Kwon et al., 2023) framework for inference. To ensure fairness, we warmed up the pipeline with 25 preliminary samples before measuring the average inference time over the next 25 samples, following the recommendation in (Zhao et al., 2024).

As shown in the Table 15, the full test-time procedure (N=16) takes roughly twice as long as single-pass baselines, which is expected since the crop-and-vote pipeline requires two inference passes. Nevertheless, by leveraging vLLM’s continuous batching capability and caching identical conditioned images and questions, our system maintains high efficiency.

In the aspect of user experience, an important strength of ReGUIDE is that its test-time scaling offers a adjustable trade-off between latency and accuracy. While the full-performance yields the highest performance at approximately 2x latency, users can choose for lighter configuration. For example, reducing the number of samples from N=16 to N=4 decreases latency by about 64% while retaining roughly 80% of the performance improvement. This flexibility suggests end-users and practitioners to control ReGUIDE’s efficiency-effectiveness trade-off based deployment. Moreover, while several recent approaches (Lian et al., 2025; Li et al., 2025) that rely on external APIs, which generate network/server-bound latency, ReGUIDE operates entirely locally, avoiding additional overhead.

C ALTERNATIVE RL POLICY OPTIMIZATION ALGORITHMS

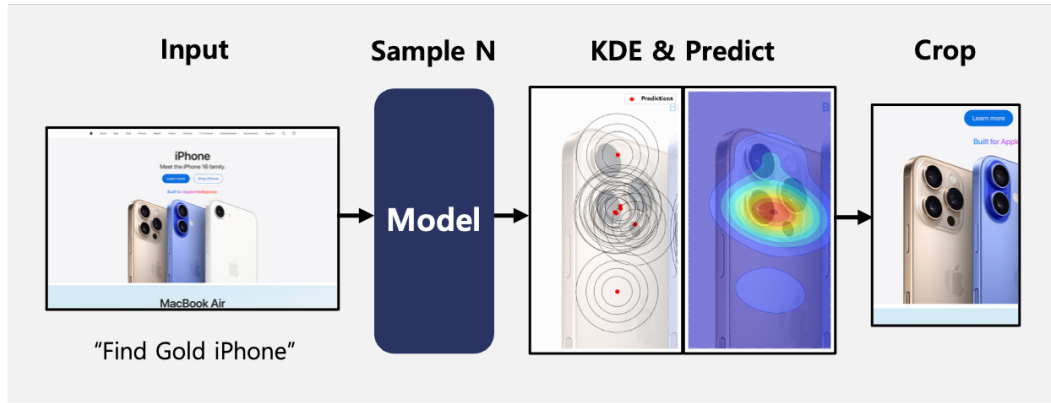
Table 16: Comparison of RL algorithms. We report accuracy (%) and average output length (Output Len.) on ScreenSpot Benchmark (Cheng et al., 2024a).

Methods	Accuracy (%)	Output Len.
REINFORCE++ (Hu, 2025)	64.8	32.3
RLOO (Ahmadian et al., 2024)	77.8	95.7
GRPO (DeepSeek, 2024)	83.3	80.8

While we primarily adopt GRPO (DeepSeek, 2024) for the learning to visual reasoning, alternative RL algorithms, such as RLOO (Ahmadian et al., 2024), REINFORCE++ (Hu, 2025), could also be considered. To verify the performance difference between RL poly optimization algorithms, we compared grounding accuracy (%) on SCREENSPOT. As shown in the Table 16, GRPO achieves the highest accuracy (83.3%), followed by RLOO (77.8%), while REINFORCE++ significantly underperforms (64.8%). Interestingly, we observed that the REINFORCE++ trained model loses its reasoning ability (i.e., shortest output length), eventually failing to generate meaningful reasoning paths.

D ILLUSTRATION OF SEARCHING STRATEGY.

1026
 1027
 1028
 1029
 1030
 1031
 1032
 1033
 1034
 1035
 1036
 1037
 1038
 1039
 1040
 1041
 1042
 1043
 1044
 1045
 1046
 1047
 1048
 1049
 1050
 1051
 1052
 1053
 1054
 1055
 1056
 1057



1058 **Figure 6: Overview of ReGUIDE’s searching strategy.** Starting from the full screenshot, the model
 1059 samples N coordinate predictions, votes using kernel density estimation, and recenters a crop on the
 1060 density peak. One searching pass is then run inside the crop, and the point with the highest KDE
 1061 density is returned as the final prediction.

1062
 1063
 1064
 1065
 1066
 1067
 1068
 1069
 1070
 1071
 1072
 1073
 1074
 1075
 1076
 1077
 1078
 1079

1080

1081 E LEARNING CURVE

1082

1083 We report the learning curve of ReGUIDE during training GRPO. The base model of the training
 1084 curve is Qwen-2.5-VL-3B. We can see that the reward is kept increasing during the training. Also,
 1085 the mean response length has decreased during the training.

1086

1087

1088

1089

1090

1091

1092

1093

1094

1095

1096

1097

1098

1099

1100

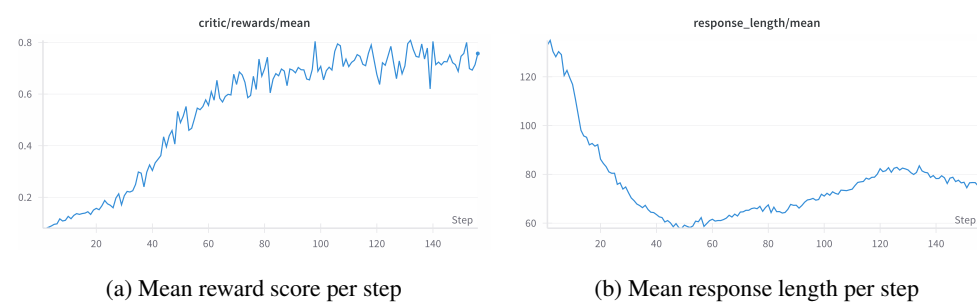


Figure 7: Learning curve during training GRPO of ReGUIDE.

1101

1102

1103

1104

1105

F PROMPTS

1106

1107

1108

1109

1110

1111

1112

1113

1114

1115

Table 17: Prompt of ReGUIDE

Element: Target element instruction.

size_x: Width of the given image.

size_y: Height of the given image.

What is the coordinate of $\{\{Element\}\}$ in the image?

The size of image is $\{\{size_x\},\{size_y\}\}$.

Output the thinking process in `<think> </think>` and final answer (coordinate (x,y)) in `<answer> </answer>` tags.

1116

Table 18: Prompt of UGround

Element: Target element instruction.

1117

1118

1119

1120

1121

1122

1123

1124

1125

1126

- Your response should aim to point to the center or a representative point within the described area/element/object as accurately as possible.

- If the description is unclear or ambiguous, infer the most relevant area or element based on its likely context or purpose.

- Your answer should be a single string (x, y) corresponding to the point of the interest.

1127

1128

1129

1130

1131

1132

1133

1134 **G GENERATION EXAMPLES**
1135

1136

1137

1138

1139

Table 19: Examples of ReGUIDE’s generated reasoning and predicted coordinate.

1140

1141

1142

1143

1144

1145

1146

1147

1148

Target Prompt: add description.

1149

1150

1151

Response: <think>To find the coordinate of [add description], I need to locate the element labeled Ädd descriptionin the image. The coordinates are given as (x, y) pairs, and I need to identify the position of this element.</think><answer>(300, 2221) </answer>

1152

1153

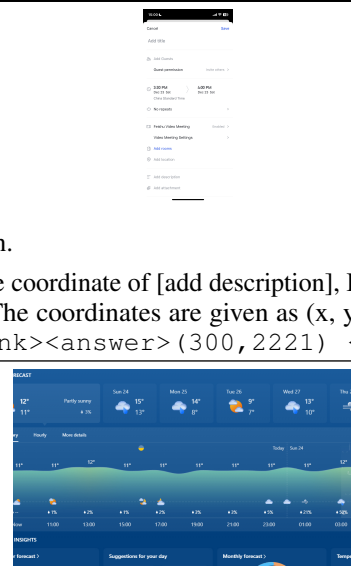
1154

1155

1156

1157

1158



1159

Target Prompt: check weather on tuesday.

1160

1161

1162

1163

Response: <think> To determine the coordinate of the iilpfolder, I need to locate it in the image and identify its position relative to the other folders. The iilpfolder is the second folder in the top row, as indicated by its position in the grid layout. </think> <answer>(584, 760)</answer>

1164

1165

1166

1167

1168

1169

1170

1171

Target Prompt: sign up for newsletter.

1172

1173

1174

1175

Response: <think> The task is to find the coordinate of the Šign Up for Newslettercheckbox in the image. The checkbox is located in the Personal Informationsection, and it is a small square with a label next to it. The coordinates are given in a specific size of the image, and we need to identify the position of the checkbox within the image. </think> <answer>(367, 85)</answer>

1176

1177

1178

1179

1180

1181

1182

1183

Target Prompt: start mapping.

1184

1185

1186

1187



1188
1189

Table 20: Failure types and their frequency from sampled generation.

1190
1191
1192
1193
1194
1195
1196

Failure Type	Number
Understand	12
Reasoning	12
Localization	6
Total	30

H FAILURE ANALYSIS

We conducted a failure analysis of sampled 30 error cases generated by ReGUIDE-3B on the ScreenSpot. Then, we categorized failure cases into 3 groups, (i) failure to understand or perceive the target, (ii) incorrect spatial reasoning, and (iii) incorrect localization. As shown in the Table 20, interestingly, 20% (=6/30) of cases are corrected in reasoning but fail to localize correctly. This highlights an important area for future work to improve localization results, followed by correct reasoning.

1205
1206
1207
1208
1209
1210
1211
1212
1213
1214
1215
1216
1217
1218
1219
1220
1221
1222
1223
1224
1225
1226
1227
1228
1229
1230
1231
1232
1233
1234
1235
1236
1237
1238
1239
1240
1241